

Characterising the complex absorber in NGC 4151

N. J. Schurch and R. S. Warwick

Department of Physics and Astronomy, University of Leicester, University Road, Leicester, LE1 7RH

ABSTRACT

We present a detailed analysis of the complex absorption apparent in the 2–6 keV X-ray spectrum of the bright nearby Seyfert galaxy NGC 4151. We first utilize the large bandpass and medium spectral resolution afforded by *BeppoSAX* data to construct a 1–100 keV spectral template, which assumes the absorption arises in both warm (*i.e.* partially photoionized) and cold gas present in the line of sight to the active nucleus of the source. Application of this spectral model to an *ASCA* “long-look” observation of NGC 4151 reveals a partial correlation between the underlying continuum flux and the ionization state of the warm absorber. Such a correlation is an intrinsic property of a warm absorber and argues strongly in favour of this interpretation for the complex absorbing column over alternative partial covering models.

The warm absorber in NGC 4151 has a column density of $\sim 2 \times 10^{23} \text{ cm}^{-2}$ with ionization parameter in the range $\log(\xi) \approx 2.4 - 2.7$. The inferred relatively low density ($\sim 10^5 \text{ cm}^{-3}$) for the warm gas, implies an equilibration timescale for the dominant ions of the same order or longer than the timescale of the continuum variability. It follows that the warm component will invariably be observed in a non-equilibrium ionization state. The warm absorber in NGC 4151 may be identified as a multi-temperature wind produced by evaporation from the inner edge of an obscuring torus as discussed in a recent paper by Krolik & Kriss (2001). The unusually complex character of the absorption seen in NGC 4151 may then be explained in terms of a fortuitous line of sight which grazes the top edge of the obscuring torus so as to intercept a substantial column of both the warm and cold gas.

We also find that (i) the reported hardening of the spectrum of NGC 4151 as the continuum level falls may be simply due to the presence of an underlying (hard and relatively constant) Compton-reflection component and (ii) the iron K α line has a relatively narrow Gaussian profile and a line flux that remains constant over both short (days) and long (months to years) timescales - a relativistically broadened iron K α feature was not required in our modelling.

Key words: galaxies: active - galaxies: Seyfert - X-rays: galaxies - galaxies: NGC 4151.

1 INTRODUCTION

The Seyfert 1 galaxy NGC 4151 was identified as an X-ray source over thirty years ago (Gursky et al. 1971). As one of the brightest Active Galactic Nuclei (AGN) accessible in the X-ray band, it has since been extensively studied by missions such as *EXOSAT*, *Ginga*, *ROSAT*, *ASCA*, *CGR*O and more recently *RXTE*, *BeppoSAX* and *Chandra*. This observational focus has revealed that the spectrum of NGC 4151 from 0.1–100 keV is comprised of a complex mixture of emission and absorption components, probably originating in a variety of locations from the innermost parts of the putative accretion disk in NGC 4151, out to the extended narrow-line region of the galaxy. Given this spectral complexity it remains to be seen whether NGC 4151 should or should

not be considered as an archetype of its class (Ulrich 2000; Zdziarski et al. 2001).

The intrinsic X-ray to γ -ray continuum emanating from the active nucleus of NGC 4151 appears to be produced by the thermal Comptonization of soft seed photons (e.g. Haardt & Maraschi 1991; Zdziarski et al. 1994, 1996, 2000; Petrucci et al. 2000). There is also a contribution from reprocessing in the form of Compton-reflection and iron-K fluorescence components (e.g. Maisack et al. 1991; Yaqoob et al. 1995; Zdziarski et al. 1996; Warwick et al. 1996; Piro et al. 2002; Zdziarski et al. 2001). Below ~ 5 keV the hard continuum is strongly cut-off by photoelectric absorption in a substantial ($N_H \sim 10^{23} \text{ cm}^{-2}$) line-of-sight gas column density (e.g. Holt et al. 1980; Yaqoob et al. 1993; Weaver et al. 1994a,b). One of the long-standing problems in X-

ray studies of NGC 4151 has been to understand the exact nature and origin of this absorption. X-ray observations show very clearly that the cut-off is not as abrupt as one might expect for absorption in a uniform slab of cold solar abundance material (i.e., the increase in opacity with decreasing photon energy is less rapid than predicted for a uniform cold absorber). Various solutions have been suggested including an inhomogeneous cold absorber (the partial covering model; Holt et al. 1980; Weaver et al. 1994b), an absorber with grossly non-solar abundances (Yaqoob & Warwick 1991) and the partial photoionization of the absorbing medium (i.e., the warm absorber model, e.g., Krolik & Kallman 1984). However, none of these has provided a really satisfactory explanation of the nature of the absorber or the processes which give rise to the large changes in the absorption apparent in NGC 4151 on timescales of days or longer (Yaqoob et al. 1989, Yaqoob et al. 1993). Unfortunately the presence of additional soft X-ray emission components which first appear at ~ 2 keV and dominate the spectrum below ~ 1 keV (Weaver et al. 1994a; Warwick, Smith & Done 1995) adds further to the complication. *EINSTEIN* and *ROSAT* HRI measurements (Elvis, Briel & Henry 1983; Morse et al. 1995) and more recently observations by *Chandra* (Ogle et al. 2000; Yang, Wilson & Ferruit 2001) have revealed that much of this soft emission emanates from a spatial resolved (~ 1.6 kpc) highly ionized plasma coincident with the optical narrow-line region of the galaxy.

In the present paper we investigate the nature of the complex X-ray absorption column in NGC 4151 and in particular focus on the question of whether at least some of the properties of the absorber can be explained in terms of photoionization effects. Our approach has been to use a high signal-to-noise *BeppoSAX* observation to define the parameters of a “spectral template” representative of the underlying continuum and other features in the X-ray spectrum of NGC 4151. We then use this template to investigate the spectral variations which occurred in NGC 4151 during a “long-look observation” carried out in the latter stages of the *ASCA* mission. The plan of the paper is as follows. In §2 we specify our spectral template model and determine the relevant spectral parameters using the *BeppoSAX* measurements. In §3 we give brief details of the *ASCA* long-look observation, outline the data reduction techniques employed and characterize the flux and spectral variability apparent in the source light curve. In the next section we describe the detailed spectral modelling of the *ASCA* data focusing on the evidence for a photoionized absorber. Finally in §5 we discuss the implications of our results.

2 THE *BeppoSAX* DATA AND THE SPECTRAL TEMPLATE

The broad bandpass of the instruments on *BeppoSAX* is a tremendous help when attempting to constrain the form of the hard X-ray spectrum of NGC 4151. During the period 1996-1999, this source was observed three times with *BeppoSAX* as reported by Piro et al. (2002). Here we utilize the observation carried out in January, 1999, which provides the best signal to noise ratio of the available datasets. X-ray data from three of the four instruments on *BeppoSAX* (namely

the LECS, MECS and PDS instruments - see Parmar et al. 1997, Boella et al. 1997, Frontera et al. 1997 respectively were obtained from the ASI Science Data Center. In the case of the LECS and MECS instruments, source spectra were preprocessed via standard *BeppoSAX* procedures using on-source extraction regions of $6'$ and $4'$ radius respectively. Standard blank-sky background files were available for the LECS and MECS whereas in the case of the PDS instrument, background-subtracted source spectra were supplied directly. The spectra were accumulated over the full observation interval (see Piro et al. 2002) to give an on-source exposure time of 83 ks in the MECS and roughly half this for the other instruments.

A BL Lac object (MS 1207.9+3945) is located $\sim 5'$ to the north of NGC 4151. Piro et al. (2002) note that its count rate is $\sim 2\%$ and $\sim 20\%$ of that of NGC 4151 in the MECS and LECS instruments respectively. The contamination of the NGC 4151 spectra will be negligible for the MECS but may, on the basis of the Piro et al. (2002) figures, be as high as $\sim 20\%$ in the LECS at ~ 1 keV. In practice the presence of this confusing source in the LECS data will have little overall impact on our spectra fitting analysis (given the relatively soft spectrum of the BLLAC - Warwick, Smith & Done 1995).

Spectral fitting was carried out using the **XSPEC V11.0.1** software package with the Sept 1997 instrument response matrices. For this purpose the source spectra were grouped to give a minimum of 20 counts per bin and the data below 1 keV (from the LECS) were excluded to avoid complications relating to the form of the soft X-ray emitting components and presence of the soft confusing source. We adopt a spectral template model which includes the following emission components:

- (i) A power-law continuum with a normalization, A_1 , and photon index, Γ , exhibiting a high-energy break at 100 keV;
- (ii) A neutral Compton-reflection component (modelled by PEXRAV in XSPEC, Magdziarz & Zdziarski 1995) with only the reflection scaling factor, R , as a free parameter. The parameters relating to the incident continuum were tied to those of the hard power-law component. In addition $\cos i$ was fixed at 0.5 and the metal abundance in the reflector was fixed at the solar value;
- (iii) An iron $K\alpha$ emission line of intensity $I_{K\alpha}$ at an energy $E_{K\alpha}$ (with an intrinsic line width $\sigma_{K\alpha}$ set to 0.1 keV);
- (iv) A second power-law continuum representative of all the additional soft X-ray emitting components with a slope coupled to that of the primary hard continuum but with a free normalization, A_2 .

As noted earlier the complex absorption in NGC 4151 has in the past been modelled in number of ways, with arguably the most successful approach being the partial covering (sometimes referred to in the literature as a dual absorber) model (e.g. Holt et al. 1980; Yaqoob & Warwick 1991; Weaver et al. 1994b). In the partial covering scenario a fraction f_{cov} of the hard continuum is absorbed by a cold gas column density $N_{H,1}$, whilst the remaining $1 - f_{cov}$ fraction of the continuum intercepts a reduced column density $N_{H,2}$. In the present paper we prefer to focus on a model employing the same number of free parameters but with the absorber stratified along the line of sight rather than perpendicular to it. In our preferred scenario the complex absorber is rep-

Table 1. The results of fitting the “spectral template” to the *BepoSAX* observation

Model Parameter	Best-Fit Value	Units
$N_{H,warm}$	$23.9^{+0.9}_{-0.9}$	10^{22} cm^{-2}
$N_{H,cold}$	$3.4^{+1.1}_{-0.8}$	10^{22} cm^{-2}
Γ	$1.65^{+0.02}_{-0.03}$	
R	$0.37^{+0.18}_{-0.15}$	
$\log(\xi)$	$2.48^{+0.06}_{-0.03}$	
A_1	$4.6^{+0.2}_{-0.2}$	$10^{-2} \text{ photon keV}^{-1} \text{ cm}^{-2} \text{ s}^{-1}$
A_2	$1.8^{+0.1}_{-0.1}$	$10^{-3} \text{ photon keV}^{-1} \text{ cm}^{-2} \text{ s}^{-1}$
$E_{K\alpha}$	$6.37^{+0.03}_{-0.02}$	keV
$I_{K\alpha}$	$3.4^{+0.4}_{-0.3}$	$10^{-4} \text{ photon cm}^{-2} \text{ s}^{-1}$
χ^2	832	
d.o.f	815	

resented as product of two absorption components, namely a warm column density $N_{H,warm}$ and a cold gas column $N_{H,cold}$. For the former we use multiplicative table models in XSPEC generated via the photoionization code XSTAR (Kallman 2001). The ionization state of the warm gas is governed by the ionization parameter $\xi = L_{ion}/n r^2$ where L_{ion} is the source luminosity in the 0.0136–13.6 keV bandpass in erg s^{-1} , n is the number of hydrogen atoms/ions in the gas per cm^{-3} and r is the distance from the central source to the inner edge of the warm cloud in cm. We assumed an ionizing continuum of the form adopted by Krolik & Kriss (1995). For further details of the photoionization modelling see Griffiths et al. (1998). The cold absorption was represented by the **wabs** model in XSPEC which is based on the absorption cross-sections tabulated in Morrison & McCammon (1983). Here we assume solar abundances in both the warm and cold absorber.

The adopted spectral model assumes that *only* the hard power-law continuum is subject to the complex absorption. However absorption arising in the line-of-sight column density through our own Galaxy is applied to all four emission components ($N_{H,Gal} = 2 \times 10^{20} \text{ cm}^{-2}$).

The results of fitting this spectral template to the *BepoSAX* data are detailed in Table 1, which lists the best fitting values for the nine free parameters of the model. The quoted errors (here as elsewhere in this paper) are at the 90% confidence level as defined by a $\Delta\chi^2=2.71$ criterion (*i.e.* assuming one interesting parameter).

The spectral template provides an excellent fit to the *BepoSAX* data as illustrated in Fig. 1. Fig. 2 shows the corresponding best-fitting model spectrum.

3 THE *ASCA* LONG-LOOK OBSERVATION

In the present paper we concentrate on the final observation of NGC 4151 carried out by *ASCA* during the period May 12–25, 2000. This was an exceptionally long observation carried out during the last phase of the *ASCA* programme, fully meriting its description as a “long-look”. The *ASCA* payload included four X-ray telescopes, two equipped with Solid-state Imaging Spectrometers (SIS) and two with Gas Imaging Spectrometers (GIS). All the relevant datasets

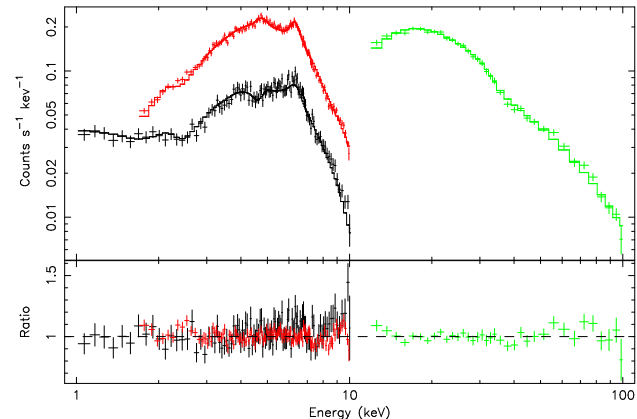


Figure 1. The *BepoSAX* LECS (black), MECS (red) and PDS (green) data fitted by our spectral template model. *Upper panel:* The count rate spectra and best-fit model. *Lower panel:* The ratio of the data to the best-fit model.

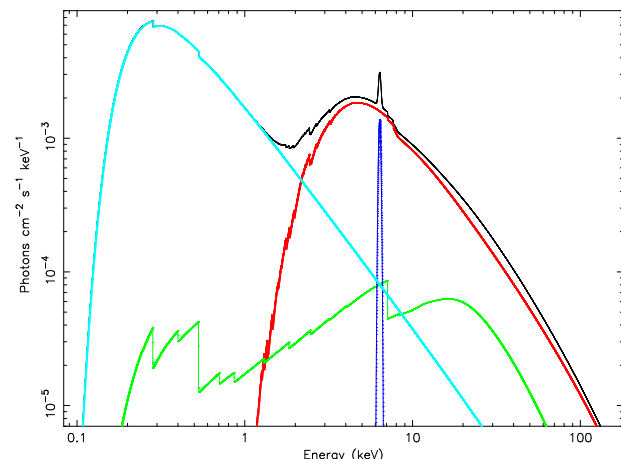


Figure 2. The spectral template model giving the best-fit to the *BepoSAX* data. There are four emission components comprising of a hard power-law continuum (red), Compton reflection (green), an iron $K\alpha$ line (dark blue) and a second power-law representing soft X-ray emitting components (light blue). Complex absorption (warm+cold components) causes the low-energy cut-off in the hard continuum. All the emission components are subject to Galactic absorption.

pertaining to the SIS and GIS instruments were obtained from the *ASCA* public archive at the HEASARC. Standard screening criteria and reduction techniques were employed using software routines within the FTOOLS package. During the long-look observation the SIS instruments were operated in a single CCD mode with the nearby BL Lac object positioned at the very edge or just off-chip in the SIS-0 and SIS-1 instruments respectively. In an attempt to reduce both the impact of the instrument background and the contamination from the BL Lac to negligible proportions, we applied a $1'$ radius source extraction circle to the SIS data. Compared to a more standard $3'$ radius extraction cell, this reduced the 1–10 keV SIS count rate by $\sim 11\%$. For the GIS data we used a $3'$ radius source extraction region and a background spectrum taken from an off-source region in the GIS field of view.

As discussed recently by Turner et al. (2001) the

ASCA SIS detectors have shown a degradation in efficiency at lower energies, which is probably due to an increased dark current levels and decreased charge transfer efficiency (CTE), producing SIS spectra which diverge from each other and from the GIS data. Furthermore, data from the last phase of *ASCA* operations (AO-8) have revealed a non-linear evolution of the SIS CTE. Here we have applied the interim solution released on 2001 February 13 by the *ASCA* GOF (in the form of the CTE file *sisph2pi_130201.fits*) which reduces some but not all of the spectral inconsistencies (see below). We restrict our analysis to the 1–10 keV band data to avoid the worst of the low energy calibration uncertainties in the SIS instruments (e.g. see Appendix A of Weaver et al. 2001). For subsequent analysis, the total accumulated on-source exposure was 285 ks in the SIS and 435 ks in the GIS detectors.

The light curve in the full 1–10 keV band is shown in Fig. 3 for the combined SIS instruments. An almost identical light curve is obtained for the combined GIS instruments demonstrating that, at least in terms of the broad band variability, the two SIS and GIS instruments produce very similar results. During the ~ 13 day observation the source shows a significant brightening by a factor of more than 3 followed by a comparable decline. The fastest variation is a flux increase of $\sim 35\%$ in roughly 12 hrs. Fig. 3 also shows a plot of the 2–5 keV/5–10 keV softness ratio versus time (for simplicity we show only the SIS data). The brightening of the source is clearly associated with a significant spectral softening, although the spectrum remains relatively soft during the subsequent decline in flux.

We have also investigated the spectral variability exhibited by NGC 4151 by calculating the fractional rms variability amplitude as a function of energy (see Edelson et al. 2002). The result, shown in Fig. 4, demonstrates, in a model independent fashion, the steep rise in the amplitude of the variability above 1 keV to a maximum at ~ 3 keV, followed a significant decline at higher energy. There is also a hint of a dip at the energy of the iron K α line (6.2–6.6 keV).

4 FITTING THE SPECTRAL TEMPLATE TO THE *ASCA* DATA

In order to study the precise nature of the spectral variability exhibited by the source, we have broken the long-look observation up into eight sections utilizing gaps in the light curve to define section boundaries as illustrated in the lower panel of Fig. 3. Appropriate response matrices and ancillary response files were constructed using standard FTOOLS routines and the spectra were again binned to a minimum of 20 counts per bin to allow the use of the χ^2 statistic in the spectral fitting.

Here our goal is to explain the softening of the spectrum as the continuum rises and the subsequent lack of spectral evolution during the continuum decline in terms of photoionization effects. In the context of the spectral template description discussed earlier, this implies changes in the ionization of the warm absorber induced by variations in the underlying continuum flux from the central source.

We adopt a very stringent requirement in spectrally fitting the *ASCA* data in that we fix *all but three* of the spectral

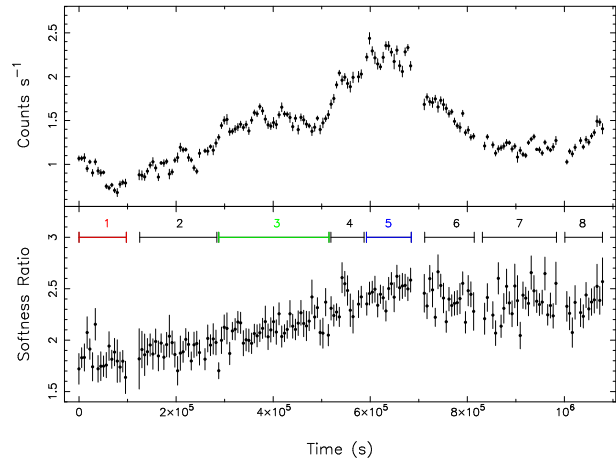


Figure 3. *Upper panel:* the combined SIS 1–10 keV X-ray light curve from the “long-look” *ASCA* observation. *Lower panel:* The variation the 2–5 keV/5–10 keV softness ratio during the observation. The horizontal bars illustrate how the observation was split into the eight time segments for the spectral analysis. The coloured horizontal bars indicate the segments for which spectra are shown in Fig. 6.

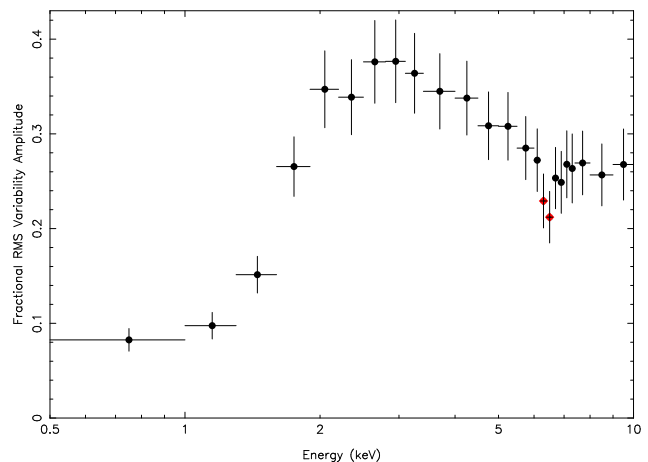


Figure 4. The fractional rms variability amplitude as a function of energy calculated for the entire *ASCA* long-look observation (SIS data).

parameters of the template model at the values derived from the *BeppeSAX* observation (Table 1). The three parameters permitted to vary are the normalization of the hard power-law continuum, A_1 , the normalization of the soft X-ray power-law, A_2 , and the ionization parameter, ξ . The column densities of the warm and cold components are kept fixed, as is the slope of the underlying continuum and the parameters of the iron K α line. For the Compton reflection, we fixed the actual component flux at the *BeppeSAX* level (rather than fixing the scale parameter R).

Before proceeding with the *ASCA* spectral analysis we need to investigate the degree of inconsistency between the SIS and GIS instruments. A comparison of the residuals when the above “template” model is fitted to the SIS-0/SIS-1 and GIS-2 spectral data from time segment 3 is shown in Fig. 5. As noted earlier these correspond to data extracted with a 1' radius source cell in the case of the SIS and a

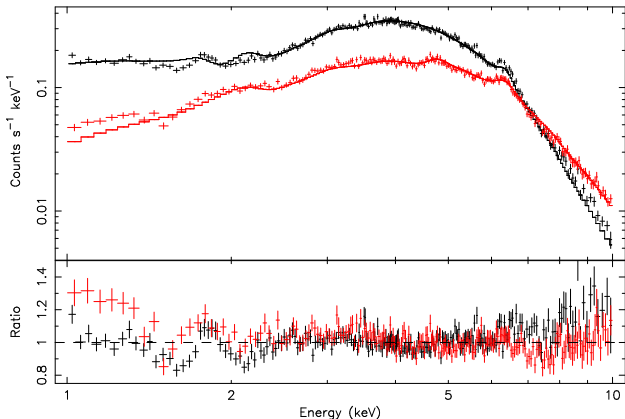


Figure 5. A comparison of the best-fitting spectral template model to the combined SIS (black) and GIS-2 (red) spectra from time segment 3 of the long-look observation. *Upper panel:* The count rate spectra and best-fit model. *Lower panel:* The ratio of the data to the best-fit model. Note the discrepancies between the SIS and GIS are most evident below ~ 1.5 keV and above 8 keV.

$3'$ radius cell for the GIS. Discrepancies between the two datasets are most evident below 2 keV and above 8 keV. The contamination of the GIS spectrum by the BL Lac appears to account for most of the problem at low energies. In fact we find that GIS data extracted within a $1'$ radius cell (thereby greatly reducing the BL Lac contribution) actually agree reasonably well with the SIS data, although this leads to a $\sim 60\%$ loss of counts in the GIS. The problem at the high energy end is similar in character to that reported by Turner et al. (2001) in a comparable *ASCA* long-look observation of the narrow-line Seyfert 1 galaxy Akn 564. Here we take a somewhat different approach to that employed by Turner et al. (2001). In the subsequent analysis we make use *solely* of the spectra derived from the SIS data. For our investigation the exclusion of the soft BL Lac flux is a useful advantage which outweighs the spectral uncertainty above 8 keV, since we employ a very tightly constrained model of the hard continuum (via the adopted spectral template). In any case, our main interest is to characterize the spectral changes rather than to determine precise values for spectral parameters. Consistency checks show that very similar results to those reported below for the SIS are obtained with the GIS instruments (in fact somewhat better reduced χ^2 are recorded) provided an extra soft component representative of the BL Lac contribution is including in the spectral modelling.

Fig. 6 compares the SIS spectra from time segments 1, 3 and 5 of the long-look observation during which the source count rate in the 1–10 keV band increased by over a factor of 3. These SIS spectra illustrate that the level of the hard continuum rises by a factor of ~ 2 and that it is the marked softening of the spectrum in the 2–6 keV band that accounts for the additional factor in the count rate increase (*cf.* Fig. 4).

The results of fitting the constrained template model to the spectra from the eight segments of the long-look observation are given in Table 2. Overall the model provides a reasonable fit to the eight spectral datasets with a combined χ^2 of 4616 for 3665 d.o.f (degrees of freedom). Interestingly the spectrally variation revealed by the long-look

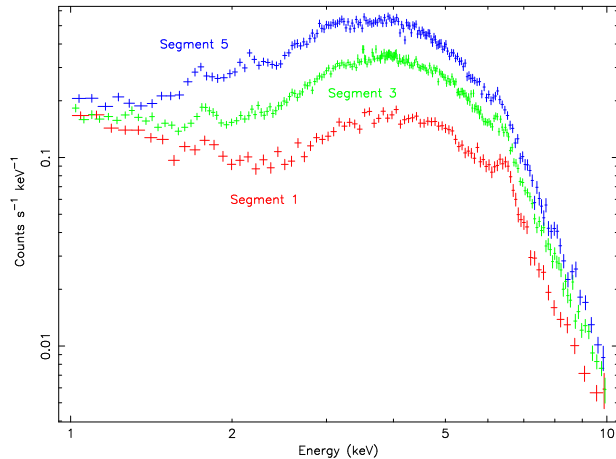


Figure 6. The 1–10 keV combined SIS spectrum of NGC 4151 as measured in three time intervals during the *ASCA* long-look observation.

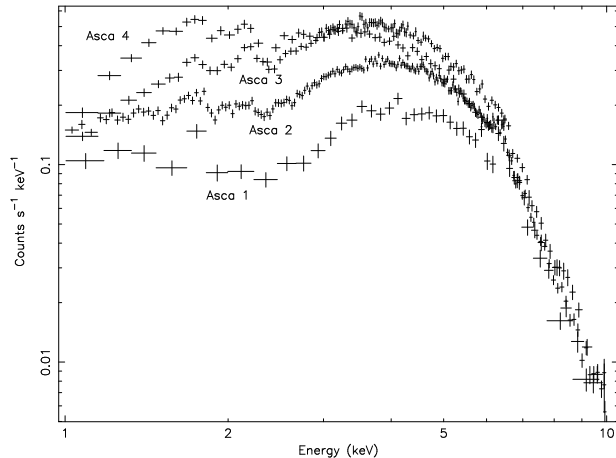


Figure 7. The 1–10 keV X-ray spectrum of NGC 4151 as measured by *ASCA* in the period 1993–1995. These are count rate spectra from the SIS-0 detector only.

data largely encompasses the range of spectral form exhibited by NGC 4151 in earlier *ASCA* observations (Fig. 7). In fact our spectral template model provides quite a good description of all the available datasets from the previous seven years of observation by both *ASCA* and *BeppoSAX*, with a range of ionization parameter not dissimilar to that derived here.

If we relax some of the parameter constraints then further improvements in the fit to the *ASCA* long-look segments can be obtained. For example, if we allow $E_{K\alpha}$ and $I_{K\alpha}$ to vary (but with the parameter value tied across the eight spectral datasets), then we obtain $\chi^2 = 4552$ for 3663 d.o.f, with best fit values of $E_{K\alpha} = 6.395 \pm 0.012$ keV and $I_{K\alpha} = 2.2_{-0.3}^{+0.2} \times 10^{-4}$ photon $\text{cm}^{-2} \text{s}^{-1}$ (which according to the F-test is significant at greater than 5 sigma). As a further step if we allow the two column density components to vary (with respect to the *BeppoSAX* values) then $\chi^2 = 4295$ for 3661 d.o.f with $N_{H,warm} = 2.0 \pm 0.1 \times 10^{23} \text{ cm}^{-2}$ and $N_{H,cold} = 4.6 \pm 0.2 \times 10^{22} \text{ cm}^{-2}$ (which is very highly significant according to the F-test). In all these fits the largest residuals are in range 1–2 keV, where the simple power-law

Table 2. Spectral fitting of the eight time segments from the *ASCA* long-look observation.

Segment	$\log(\xi)$	A_1 ^a	A_2 ^b
1	$2.483^{+0.009}_{-0.009}$	$1.99^{+0.04}_{-0.04}$	$0.82^{+0.03}_{-0.03}$
2	$2.513^{+0.007}_{-0.005}$	$2.58^{+0.04}_{-0.04}$	$0.80^{+0.02}_{-0.02}$
3	$2.554^{+0.006}_{-0.002}$	$3.79^{+0.03}_{-0.05}$	$0.85^{+0.02}_{-0.03}$
4	$2.615^{+0.004}_{-0.013}$	$4.59^{+0.10}_{-0.01}$	$0.85^{+0.07}_{-0.02}$
5	$2.644^{+0.001}_{-0.011}$	$5.25^{+0.08}_{-0.01}$	$0.87^{+0.06}_{-0.01}$
6	$2.636^{+0.003}_{-0.009}$	$3.50^{+0.05}_{-0.03}$	$0.88^{+0.03}_{-0.01}$
7	$2.630^{+0.004}_{-0.009}$	$2.42^{+0.03}_{-0.02}$	$0.93^{+0.03}_{-0.03}$
8	$2.643^{+0.006}_{-0.008}$	$2.51^{+0.04}_{-0.03}$	$0.94^{+0.04}_{-0.04}$

^a 10^{-2} photon keV $^{-1}$ cm $^{-2}$ s $^{-1}$ at 1 keV.

^b 10^{-3} photon keV $^{-1}$ cm $^{-2}$ s $^{-1}$ at 1 keV.

model of the soft emission components is clearly a gross over-simplification (Ogle et al. 2000). However, the presence of these 1-2 keV residuals is very unlikely to influence our interpretation of the observed spectral variations in terms of a variable warm absorber (see below).

The spectral fitting of the *ASCA* long-look observation reveals a range of ionization states for the warm absorber in NGC 4151 (Table 2). A clear correlation is apparent between the ionization parameter (ξ) and the level of the hard continuum (A_1) for the first five segments of the observation, which correspond to the period of increasing flux in the light curve (Fig 8). However as the flux drops (segments 6-8) the correlation is lost and the ionization state remains at a comparable level to that seen at the peak of the lightcurve. In contrast, in the *BeppeSAX* observation, although the continuum was at a level comparable to that at the peak of *ASCA* light curve, in this case the ionization of the warm absorber was at the bottom end of the range observed with *ASCA* (Fig 8). The observed correlation in the *ASCA* long-look data lends support to the warm absorber interpretation for the observed absorbing column and we argue in §5 that the lack of a sustained correlation between ionization level and the continuum flux, is not necessarily inconsistent with this description.

The normalization of the soft power-law component, A_2 , varies by $\sim 15\%$ during the *ASCA* long-look observation. There is also an apparent factor 2 decline in the soft component over the 18 month interval between the *BeppeSAX* and *ASCA* observations, although as noted earlier there may be some preferential contamination of the *BeppeSAX* data by the nearby BL Lac object. Bearing in mind that much of the soft emission in NGC 4151 originates in the spatially extended component recently imaged by *Chandra*, (Ogle et al. 2000; Yang et al. 2001), these results would suggest that there may be some leakage of the hard continuum flux through the absorber down to ~ 1 keV (as suggested by Fig 4) whereas in the current spectral modelling the cut-off is nearer to 2 keV (see Fig 2). Since the complex absorption in NGC 4151 is likely to arise from gas exhibiting a range of ionization parameters, our two component (cold + warm gas) model must, at best, represent only a rough approximation to the real system.

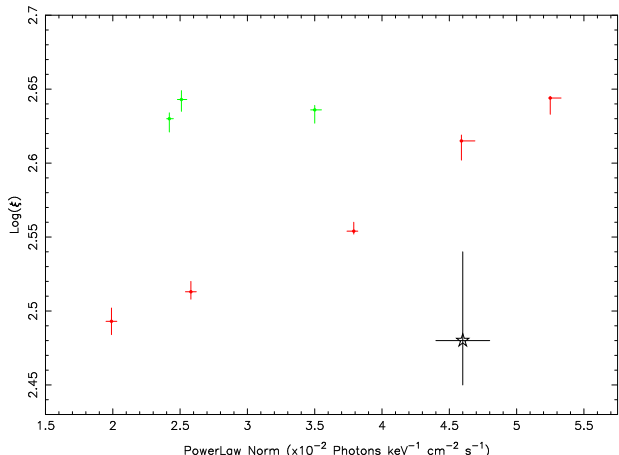


Figure 8. Correlation between ionization parameter (ξ) and the normalization of the hard power-law continuum for the eight segments of the *ASCA* “long-look” observation. The red points mark the segments where the lightcurve is rising, the green points mark the segments where the lightcurve is falling. The point marked by the star symbol is from the *BeppeSAX* observation; the error bar is larger in this case due to the additional free parameters in the spectral fitting.

5 DISCUSSION

5.1 The physical state of the photoionized absorber in NGC 4151

One of the major advantages of the warm absorber description is that it is based on a physical model which is, in principle, readily testable. For example, given sufficient spectral resolution, sensitivity and dynamic range, the true ionization state of the warm gas can be determined directly from the absorption edges present in the X-ray spectrum. A further key diagnostic, somewhat more in tune with current measurement capabilities in the case of heavily absorbed sources such as NGC 4151, is that ionization parameter of the warm gas should track the intensity of the ionizing radiation field, albeit in a complex fashion (Nicastro et al. 1999). In contrast the popular partial covering (or dual absorber) models are based on rather arbitrary, constructed geometries which are very difficult to verify.

Previous studies of NGC 4151 have failed to demonstrate in an unambiguous fashion that the absorbing medium in NGC 4151 does respond to changes in the level of the incident hard continuum (Yaqoob et al. 1989; Fiore et al. 1990; Warwick et al. 1996; Piro et al. 2002). However, the *ASCA* long-look observation provides an excellent opportunity to study the response of the absorber to continuum changes. The correlation between ionization parameter and the level of the hard continuum apparent over the rising part of the light curve (Fig. 8) would appear to be the signature of a partially photoionized medium. However, a problem then presents itself in that the relatively high ionization state is maintained over the latter part of the observation despite the decline in the continuum. A possible explanation for this behaviour is that the timescale on which significant continuum variations are occurring ($\sim 3 \times 10^5$ s) is somewhat shorter than the timescale on which the balance between photoionization and recombination can be re-established in the plasma. The result is that with quasi-continuous contin-

uum variations (of which the light curve in Fig. 3 represents only a brief snapshot) the warm absorber is invariably in a non-equilibrium ionization state. Nicastro et al. (1999) have discussed some of the complications which arise in such circumstances and show that the delayed response of a medium to sharp increases and decreases in the incident ionizing flux can give rise to variations in the ionization state apparently unconnected with flux changes (and even anti-correlations of ionization level with flux). In the case of NGC 4151 there is clear evidence that the medium is slow to respond; for example even during the period when the ionization parameter and the continuum show a correlation, the former changes by a factor 1.8 compared to a factor of 2.5 for the latter. However, the fact that the degree of ionization tracks the light curve better during the rising segment than during the decline is consistent with the fact that $T_{ion} \propto L_{ion}^{-1}$, as is evident from Fig. 1 of Nicastro et al. (1999).

The parameter values for the warm absorber in NGC 4151 are not too far removed from one of the standard cases considered by Krolik & Kriss (2001) (although the assumed form of underlying continuum is somewhat modified with respect to the version in Krolik & Kriss et al. (1995), which we have adopted in the present work). For example, taking $\xi = 300$ and $L_{ion} = 10^{44} \text{ erg s}^{-1}$ as representative values for the warm absorber in NGC 4151 and taking the distance of the warm medium from the continuum source to be 1 pc, then the inferred gas density is $n \approx 4 \times 10^4 \text{ cm}^{-3}$. Table 1 in Krolik & Kriss (2001) gives the corresponding equilibration timescales for selected ions in such a plasma. The warm absorber cut-off is best measured between 2–6 keV, where absorption edges due to the hydrogen- and helium-like ions of Mg, Si, S, Ar and Ca will be of importance (although not individually resolvable in the *ASCA* data). For these ions the relevant equilibration timescales are typically between $1 - 8 \times 10^6 \text{ s}$. In fact, the measured column density for the warm absorber in NGC 4151 of $\sim 2 \times 10^{23} \text{ cm}^{-2}$ implies $r_{max} \sim 0.5 \text{ pc}$ (Krolik & Kriss 2001), which in turn (since $t_{ion} \propto r^2$), requires a factor 4 reduction in the equilibration timescales quoted by Krolik & Kriss. Nevertheless it is still true that the variability timescale in NGC 4151 is short enough for the warm absorber to be out of ionization equilibrium as required. Since different ions reach their equilibrium abundance, for a given flux of ionizing radiation, on different timescales, the detailed form of the absorption cut-off will depend on the luminosity history of the source stretching back over a period equal to the longest relevant equilibration timescale, which in NGC 4151 will be $\sim 10^7 \text{ s}$.

5.2 The properties of the iron $K\alpha$ line

In the present paper we have modelled the iron $K\alpha$ emission in a very simple fashion, namely as a single narrow line at an energy appropriate to cold (*i.e.* neutral or low-ionization) material. In the long-look *ASCA* observation, the measured line flux was $2.2_{-0.3}^{+0.2} \times 10^{-4} \text{ photon cm}^{-2} \text{s}^{-1}$, with no evidence for any variations in either the line intensity or in the line profile during the observation period. The *BepiSAX* observation gave a somewhat higher value (at the 3σ level) suggesting the possibility of line variations, but on the other hand the *ASCA* value is in excellent agreement with the iron $K\alpha$ line flux measured by *Ginga* almost ten years earlier. The lack of significant variability on timescales of

many years suggests the origin of this narrow component is in a medium located well outside of the immediate surroundings of the nuclear source (*i.e.* not in a putative accretion disk), but probably does not exclude the region occupied by the warm absorber. However, the predicted range of iron ionization states in the warm medium is Fe XVI – FeXXI with the associated $K\alpha$ line emission ranging in energy from 6.4 – 6.6 keV. Since the measured line energy excludes much of this range, we conclude that the bulk of the line equivalent width (which ranges from 82 – 195 eV during the eight segments of the observation, depending on the continuum level) derives from less strongly photoionized material located further from the nucleus than the warm medium. The cold absorber in our model can only account for the observed iron $K\alpha$ flux if it subtends a full 4π steradians as viewed from the central source and has an iron abundance a factor 3 higher than solar.

In contrast with previous claims suggesting a complex broad iron line structure in NGC 4151 (Yaqoob, et al. 1995; Wang et al. 1999, 2001; Yaqoob, et al. 2001), we find no compelling evidence to include a relativistically broadened line in any of our modelling (the best fit intrinsic line width of the “narrow” line in the *ASCA* data was $110 \pm 20 \text{ eV}$ but this may over estimate the true line width given the SIS calibration uncertainties). The lack of any variability in the line profile during the observation contrasts with earlier claims of line profile variability in NGC 4151 on 10^4 s timescales (Wang et al. 2001).

Clearly a very extended broad-line profile is easily confused with a continuum form including a non-negligible contribution from Compton reflection and modified by a complex absorption. The complex variable nature of the underlying continuum and the absorption may then easily manifest itself as variability in the broad-line profile. We will return to this issue at a later date utilizing newly acquired data from *XMM-Newton*.

5.3 The spectral index versus flux correlation

Previous observations of NGC 4151 with both *EXOSAT* and *Ginga* have revealed an apparent correlation between spectral index measured in the 2–10 keV band and the level of the underlying continuum (Perola et al. 1986; Yaqoob & Warwick 1991; Yaqoob et al. 1993). Fig. 9 shows a compilation of measurements from *EXOSAT* and *Ginga* (taken from Yaqoob et al. 1993) which suggests that as the source brightens the photon index steepens, from $\Gamma \sim 1.35$ to $\Gamma \sim 1.7$, at which point the correlation saturates. Yaqoob et al. (1993) also note that the spectral slope changes occur on roughly the same timescale as the flux variations. However, a perplexing aspect of the spectral index flux correlation observed in the medium energy bandpass is that the effect is not mirrored in the hard X-ray/soft gamma regime (Johnson et al. 1997; Piro et al. 2002).

An underlying assumption of the spectral template model adopted in the present paper is that the spectral index of the hard power-law continuum in NGC 4151 remains constant (at a value $\Gamma \approx 1.65$), as the continuum flux changes, in apparent contradiction to the correlation noted above. (Testing this assumption against the *ASCA* observation demonstrates that the *ASCA* datasets are broadly consistent with the assumed value of $\Gamma=1.65$, however the

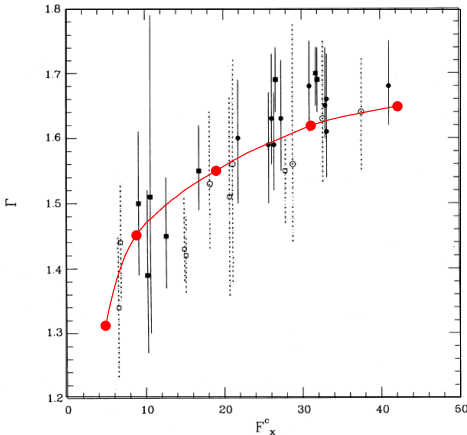


Figure 9. Measurements of the spectral photon index versus the absorption-corrected 2–10 keV flux from *EXOSAT* and *Ginga* observations, taken from Fig. 2 of Yaqoob et al. (1993). The solid curve represents the results of a simulation in which a constant Compton-reflection component was included along with a power-law continuum with a variable normalization but fixed slope (*i.e.*, $\Gamma = 1.65$). See the text for further details.

values are poorly constrained due to the very limited effective bandpass, and the fact that the values of Γ derived are very dependent on the exact details of the applied spectral model).

We have investigated the possibility that the spectral index versus relation may actually be a misinterpretation of the softening of the NGC 4151 spectrum as the source flux increases, bearing in mind that the reported correlation was established using both proportional counter data with limited spectral resolution and a highly simplified spectral model (in fact just a power-law continuum model, modified by a heavy cold absorbing column). To this end we have taken our spectral template model and an appropriate *Ginga* response, and simulated a set of five *Ginga* spectra using XSPEC. In this simulation, the normalization of the hard power-law continuum was increased in steps from 1 to 10×10^{-2} photons $\text{cm}^{-2} \text{s}^{-1}$, but with all the other parameter values, (including the ionization parameter and the *flux* in the Compton-reflection component) frozen at the values obtained from the *BeppoSAX* spectral fitting. The simulated 3.5–20 keV *Ginga* spectra were then each fitted with a simple absorbed power-law model (*cf.* Yaqoob & Warwick 1991; Yaqoob et al. 1993) and the effective photon spectral index measured. The result was a spectral index versus 2–10 keV flux correlation closely matching the reported correlation (Fig. 9). Since the simulation did not include any of the complications associated with varying ionization parameter of the warm absorber, it follows that the observed spectral changes are induced solely as a result of the presence of a non-varying spectrally-hard Compton-reflection component. Clearly, in this scenario, as the direct continuum brightens, the relative contribution of the Compton-reflection declines and the overall spectrum softens until eventually the measured spectral index saturates at the value pertaining to the underlying continuum.

6 CONCLUSION

There has been much debate as to whether NGC 4151 is simply a very bright, nearby representative of the broad class of galaxies harbouring luminous Seyfert nuclei or a unique object (Ulrich 2000). In the X-ray band this uncertainty is due, in large measure, to the heavy, complex and variable absorption which characterizes the 2–6 keV spectrum of NGC 4151 but which is not mirrored in the great majority of well-studied Seyfert galaxies (Mrk 6 is arguably the best known example of a NGC 4151 analogue, Feldmeier et al. 1999).

In this paper we have presented a detailed analysis of two archival datasets of NGC 4151, one from *BeppoSAX* the other from *ASCA*, which tests the hypothesis that the complex absorption is due to a combination of warm and cold gas distributed along the line of sight to the active Seyfert nucleus in this source. We find that this relatively simple model does indeed provide a good description of the two datasets in question and, in fact, gives a reasonable fit to all of the *ASCA* and *BeppoSAX* observations from the past seven years. Our key finding is that the warm absorber corresponds to a relative low density ($\sim 10^5 \text{ cm}^{-3}$) gas, with a column density of $\sim 2 \times 10^{23} \text{ cm}^{-2}$ and with ionization parameter in the range $\log(\xi) \approx 2.4 - 2.7$. Since the equilibration timescale for the dominant ions is of the same order or longer than the timescale of the continuum variability, the warm component is invariably observed in a non-equilibrium ionization state. Non-equilibrium conditions help explain why past studies based on relatively short observations spaced by weeks, months or years have failed to identify a consistent signature of the warm absorber in this source.

In a recent paper, Krolik & Kriss (2001) discuss how evaporation from the inner edge of the obscuring torus in an AGN can give rise to an inhomogeneous photoionized wind in which a broad range of temperatures coexist in equilibrium. Krolik & Kriss (2001) then go on to suggest that this wind is the origin of the highly ionized, warm absorbers seen in over half of type 1 Seyfert galaxies. For most Seyfert 1 galaxies the properties of the warm absorber are inferred from the OVII and OVIII absorption edges, whereas in NGC 4151 the combination of warm and cold absorbers gives rise to a sharp spectral cutoff below ~ 2 keV, thus eliminating the oxygen features. Nevertheless, as noted earlier, the inferred properties of the warm component in NGC 4151 are not too far removed from one the standard cases detailed by Krolik & Kriss (2001). It is therefore reasonable to hypothesise that the warm absorber in NGC 4151 originates in such a multi-temperature wind, but that the unusually complex character of the absorption is due to a line of sight which grazes the top edge of the obscuring torus so as to intercept a substantial column of *both* the warm and cold components. In essence in terms of its X-ray absorption properties, NGC 4151 is intermediate between the Seyfert galaxies in which the absorption, if present, is predominantly due to the Krolik & Kriss's multi-temperature wind (type 1 objects) and those where the cooler material of the obscuring torus dominates (type 2 objects).

The other findings of this paper are that (i) the reported hardening of the spectrum of NGC 4151 as the continuum level falls may be simply due to the presence of an underlying (hard and relatively constant) Compton-reflection component and (ii) there is no compelling evidence for a rela-

tistically broadened iron K α line in NGC 4151 contrary to earlier claims.

In summary, it appears that many of the X-ray properties of NGC 4151 can be explained in terms of the current paradigm for Seyfert galaxies. Future observations with *XMM-Newton*, *Chandra* and *INTEGRAL* will be able to test the degree to which our spectral template description is valid and should further illuminate the question of whether NGC 4151 should be regarded as the archetypal Seyfert galaxy.

ACKNOWLEDGMENTS

NJS gratefully acknowledges the financial support from PPARC. It is a pleasure to thank Simon Vaughan for his many valuable discussions, and Keith Arnaud for his help with XSPEC. The archival *ASCA* X-ray data used in this work was obtained from the Leicester Database and Archive Service (LEDAS) at the Department of Physics & Astronomy, University of Leicester. The archival *BepoSAX* X-ray data used in this work was obtained from the *BepoSAX* ASI Science Data Center at ESRIN, Italy. This research has made extensive use of NASA's Astrophysics Data System Abstract Service.

REFERENCES

Boella G., Chiappetti L., Conti G., Cusumano G., del Sordo S., La Rosa G., Maccarone M. C., Mineo T., Molendi S., Re S., Sacco B., Tripiciano M., 1997, *A&AS*, 122, 327

Edelson R., Turner T. J., Pounds K., Vaughan S., Markowitz A., Marshall H., Dobbie P., Warwick R., 2002, *astro-ph/0108387*

Elvis M., Briel U. G., Henry J. P., 1983, *ApJ*, 268, 105

Feldmeier J.J., Brandt W.N., Elvis M., Fabian A.C., Iwasawa K., Mathur S., 1999, *ApJ*, 510, 167

Fiore F., Perola G. C., Romano M., 1990, *MNRAS*, 243, 522

Frontera F., Costa E., dal Fiume D., Feroci M., Nicastro L., Orlandini M., Palazzi E., Zavattini G., 1997, *A&AS*, 122, 357

Griffiths R. G., Warwick R. S., Georgantopoulos I., Done C., Smith D. A., 1998, *MNRAS*, 298, 1159

Gursky H., Kellogg E. M., Leong C., Tananbaum H., Giacconi R., 1971, *ApJ*, 165, L43

Haardt F., Maraschi L., 1991, 380, L51

Holt S. S., Mushotzky R. F., Boldt E. A., Serlemitsos P. J., Becker R. H., Szymkowiak A. E., White N. E., 1980, *ApJL*, 241, L13

Johnson W. N., McNaron-Brown K., Kurfess J. D., Zdziarski A. A., Magdziarz P., Gehrels N., 1997, *ApJ*, 482, 173

Kallman T. R., 2001, <http://heasarc.gsfc.nasa.gov/docs/software/xstar/docs/html/xstarmanual.html>

Krolik J. H., Kallman T. R., 1984, *ApJ*, 286, 366

Krolik J. H., Kriss G. A., 1995, *ApJ*, 447, 512

Krolik J. H., Kriss G. A., 2001, *ApJ*, 561, 684

Magdziarz P., Zdziarski A. A., 1995, *MNRAS*, 273, 837

Maisack M., Yaqoob T., 1991, *A&A*, 249, 25

Morrison R., McCammon D., 1983, *ApJ*, 270, 119

Morse J. A., Wilson A. S., Elvis M., Weaver K. A., 1995, *ApJ*, 439, 121

Nicastro F., Fiore F., Perola G. C., Elvis M., 1999, *ApJ*, 512, 184

Ogle P. M., Marshall H. L., Lee J. C., Canizares C. R., 2000, *ApJL*, 545, L81

Parmar A. N., Martin D. D. E., Baudz M., Favata F., Kuulkers E., Vacanti G., Lammers U., Peacock A., Taylor B. G., 1997, *A&AS*, 122, 309

Perola G. C., Piro L., Altamore A., Fiore F., Boksenberg A., Penston M. V., Snijders M. A. J., Bromage G. E., Clavel J., Elvius A., Ulrich M. H., 1986, *ApJ*, 306, 508

Petrucci P. O., Haardt F., Maraschi L., Grandi P., Matt G., Nicastro F., Piro L., Perola G. C., De Rosa A., 2000, *ApJ*, 540, 131

Piro L., Nicastro F., Perola G. C., Capalbi M., Cappi P., Grandi P., Maraschi L., Petrucci P. O., 2002, *A&A*, in preparation.

Turner T. J., Romano P., George I. M., Edelson R., Collier S. J., Mathur S., Peterson B. M., 2001, *ApJ*, 561, 131

Ulrich M.-H., 2000, *A&ARv*, 10, 135

Wang J., Zhou Y., Wang T., 1999, *ApJL*, 523, L129

Wang J., Wang T., Zhou Y., 2001, *ApJ*, 549, 891

Warwick R. S., Smith D. A., Done C., 1995, *MNRAS*, 275, 1003

Warwick R. S., Smith D. A., Yaqoob T., Edelson R., Johnson W. N., Reichert G. A., Clavel J., Magdziarz P., Peterson B. M., Zdziarski A. A., 1996, *ApJ*, 470, 349

Weaver K. A., Mushotzky R. F., Arnaud K. A., Serlemitsos P. J., Marshall F. E., Petre R., Jahoda K. M., Smale A. P., Netzer H., 1994a, *ApJ*, 423, 621

Weaver K. A., Yaqoob T., Holt S. S., Mushotzky R. F., Matsuoka M., Yamauchi M., 1994b, *APJL*, 436, L27

Weaver K. A., Gelbord J., Yaqoob T., 2001, *ApJ*, 550 261

Yaqoob T., Warwick R. S., Pounds K. A., 1989, *MNRAS*, 236, 153

Yaqoob T., Warwick R. S., 1991, *MNRAS*, 248, 773

Yaqoob T., Warwick R. S., Makino F., Otani C., Sokoloski J. L., Bond I. A., Yamauchi M., 1993, *MNRAS*, 262, 435

Yaqoob T., Edelson R., Weaver K. A., Warwick R. S., Mushotzky R. F., Serlemitsos P. J., Holt S. S., 1995, *ApJL*, 453, L81

Yaqoob T., Padmanabhan U., Dotani T., Nandra K., 2001, *astro-ph/0112318*

Yang Y., Wilson A. S., Ferruit P., 2001, *ApJ*, 563, 124

Zdziarski A. A., Fabian A. C., Nandra K., Celotti A., Rees M. J., Done C., Coppi P. S., Madejski G. M., 1994, *MNRAS*, 269, L55

Zdziarski A. A., Johnson W. N., Magdziarz P., 1996, *MNRAS*, 283, 193

Zdziarski A. A., Poutanen J., Johnson W. N., 2000, *ApJ*, 542, 703

Zdziarski A. A., Leighly K. M., Matsuoka M., Cappi M., Mihara T., 2002, *ApJ*, 573